

# FUSIONFORMER: A MULTI-SENSORY FUSION IN BIRD’S-EYE-VIEW AND TEMPORAL CONSISTENT TRANSFORMER FOR 3D OBJECT DETECTION

Chunyong Hu<sup>1\*</sup>, Hang Zheng<sup>1\*</sup>, Kun Li<sup>1</sup>, Jianyun Xu<sup>1</sup>, Weibo Mao<sup>1</sup>, Maochun Luo<sup>1</sup>,

Lingxuan Wang<sup>1</sup>, Mingxia Chen<sup>1</sup>, Qihao Peng<sup>1</sup>, Kaixuan Liu<sup>1</sup>, Yiru Zhao<sup>1</sup>, Peihan Hao<sup>1</sup>,

Minzhe Liu<sup>1</sup>, Kaicheng Yu<sup>1,2§</sup>

## ABSTRACT

Multi-sensor modal fusion has demonstrated strong advantages in 3D object detection tasks. However, existing methods that fuse multi-modal features require transforming features into the bird’s eye view space and may lose certain information on Z-axis, thus leading to inferior performance. To this end, we propose a novel end-to-end multi-modal fusion transformer-based framework, dubbed FusionFormer, that incorporates deformable attention and residual structures within the fusion encoding module. Specifically, by developing a uniform sampling strategy, our method can easily sample from 2D image and 3D voxel features spontaneously, thus exploiting flexible adaptability and avoiding explicit transformation to the bird’s eye view space during the feature concatenation process. We further implement a residual structure in our feature encoder to ensure the model’s robustness in case of missing an input modality. Through extensive experiments on a popular autonomous driving benchmark dataset, nuScenes, our method achieves state-of-the-art single model performance of 72.6% mAP and 75.1% NDS in the 3D object detection task without test time augmentation.

## 1 INTRODUCTION

Autonomous driving technologies typically rely on multiple sensors for safety considerations, such as LiDAR (Chen et al., 2023; Yin et al., 2021; Wang et al., 2020; Lang et al., 2019), cameras (Wang et al., 2021b; 2022), and radar (Meyer & Kuschik, 2019; Meyer et al., 2021). These sensors possess distinct characteristics. For example, LiDAR can provide accurate yet sparse point clouds with 3D information, while images have dense features but lack such depth information. To enhance performance, multi-modal fusion can be used to integrate the strengths of these sensors. By combining information from multiple sensors, autonomous driving systems can achieve better accuracy and robustness, making them more reliable for real-world applications. Concatenating multi-modality features via simple concatenation in bird’s eye view (BEV) space becomes a defacto standard to achieve state-of-the-art performance. As shown in Figure 1, current fusion framework fuses features from LiDAR point cloud and images in BEV space via simple concatenation (Liu et al., 2023; Liang et al., 2022) or a certain transformer architecture (Yan et al., 2023). However, we conjecture that these approaches has certain two limitations.

In order to fuse information at BEV level, we must first transform the 2D image features into 3D via certain geometry view transformation (Pillion & Fidler, 2020). This process requires using a monocular depth estimation module which is an ill-posed problem and can generate inaccurate feature alignment. We believe that a superior approach is to exploit features from sparse point cloud

\*Equal Contribution. §Corresponding Author.

<sup>1</sup> Autonomous Driving Lab, Cainiao Network, China

<sup>2</sup> Autonomous Intelligence Lab, Westlake University, China  
Email:kyu@westlake.edu.cn

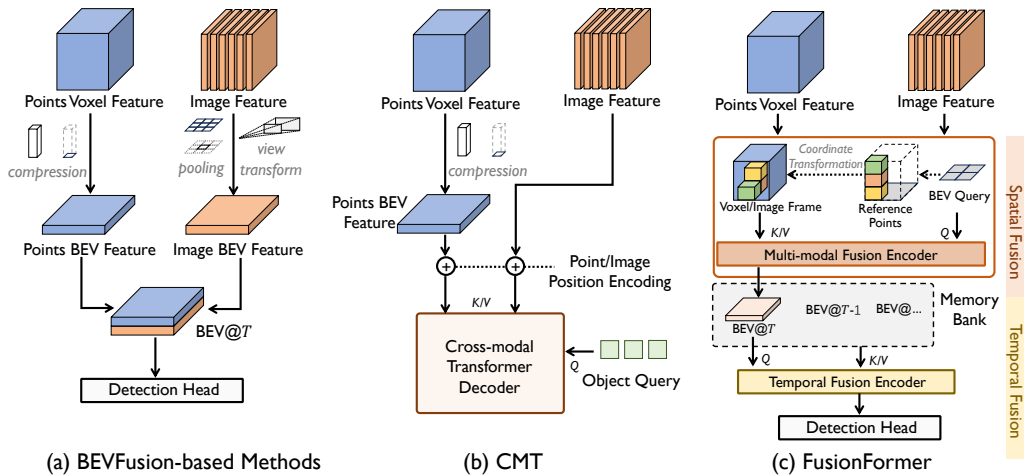


Figure 1: **Comparison between state-of-the-art methods and our FusionFormer.** (a) In BEVFusion-based methods, the camera features and points features are transformed into BEV space and fused with concatenation. (b) In CMT, the points voxel features are first compressed into BEV features, then are encoded with the same positional encoding as image features. Then, each object query is passed into a transformer decoder to generate the prediction result. (c) In FusionFormer, the fusion of multi-modal features is achieved by sequentially interacting BEV queries with original point cloud voxel features and image features. This interaction leverages the depth references provided by point cloud features for the view transformer of image features, while the image features complement the sparsity of point cloud features. As a result, more accurate and dense fused BEV representations are obtained. Additionally, FusionFormer incorporates a temporal fusion encoding module, enabling the fusion of BEV features from historical frames.

to assist this process. Concurrently, Yan et al. (2023) proposes a transformer to leverage positional encoding to encode image features, which can be viewed as an alternative approach to alleviate this issue. However, all aforementioned methods explicitly transform the point voxel features into BEV space before the fusion module by compressing the Z-axis dimensional features into vectors. This may hinder the performance of downstream tasks that involves height information, such as 3D object detection where one needs to predict the height of the bounding box.

To tackle above problems, we propose a novel multi-modal fusion framework for 3D object detection, dubbed FusionFormer to address these challenges. As shown in Figure 1 (c), FusionFormer can generate fused BEV features by sequentially fusing LiDAR and image features with deformable attention (Zhu et al., 2020), which inherently samples features at the reference points corresponding to the BEV queries. By developing a uniform sampling strategy, our FusionFormer can easily sample from 2D image and 3D voxel features at the same time thus exhibits flexible adaptability across different modality inputs, and avoids explicit transformation and the need of monocular depth estimation. As a result, multi-modal features can be input in their original forms avoiding the information loss when transforming into BEV features. During the fusion encoding process, the point cloud features can serve as depth references for the view transform of image features, while the dense semantic features from images reciprocally complement the sparsity of point cloud features, leading to the generation of more accurate and dense fused BEV features. Notably, the multi-modal fusion encoder incorporates residual structures, ensuring the model’s robustness in the presence of missing point cloud or image features. We also propose a plug-and-play temporal fusion module along with our FusionFormer to support temporal fusion of BEV features from previous frames.

In addition, to verify the effectiveness and flexibility of our approaches, we use voxel features obtained from monocular depth estimation of only images to replace the features obtained from LiDAR point clouds to construct a FusionFormer that only uses camera modality.

In summary, we present the following contributions in this paper:

- 
- We notice that state-of-the-art multi-modality frameworks need explicitly compressing the voxel features into BEV space before fusing with image features might lead to inferior performance, and propose a novel transformer based framework with a uniform sampling strategy to address this issue.
  - We also demonstrate that our method is flexible and can be transformed into a camera only 3D object detector by replacing the LiDAR features to image features with monocular depth estimation.
  - Our method achieves state-of-the-art single model performance of 72.6% mAP and 75.1% NDS in the 3D object detection task of the nuScenes dataset without test time augmentation.

## 2 RELATED WORK

**Visual-centric 3D Object Detection.** In recent years, camera-based 3D object detection has gained increasing attention in the field of autonomous driving. Early approaches relied on predicting the 3D parameters of objects based on the results of 2D object detection (Park et al., 2021; Wang et al., 2021b). Recently, BEV-based 3D object detection has become a hot research topic (Xie et al., 2022). Compared to previous methods, BEV-based 3D object detection can directly output 3D object detection results around the vehicle using multi-view camera images, without requiring post-processing of detection results in overlapping regions. Inspired by LSS (Phillion & Fidler, 2020), recent works like BEVDet (Huang et al., 2021) and BEVDepth (Li et al., 2023) have used bin-based depth prediction to transform multi-view camera features into BEV space. PETR (Liu et al., 2022a) achieves a camera-based BEV method with transformer by adding 3D position encoding. DETR3D (Wang et al., 2022) and BEVFormer (Li et al., 2022c) use deformable attention to make the query under BEV space interact with local features related to its position projection range during the transformer process, achieving the transformation from multi-view camera space to BEV space.

**LiDAR-centric 3D Object Detection.** LiDAR-based 3D object detection methods can be categorized into different types based on the representation form of point cloud features. Point-wise methods extract features directly from individual points and output 3D object detection results end-to-end (Qi et al., 2018; Paigwar et al., 2019). BEV-based methods, on the other hand, construct intermediate feature forms before transforming them into BEV space (Yin et al., 2021). For instance, VoxelNet (Zhou & Tuzel, 2018) voxelizes the raw point cloud and applies sparse 3D convolutions to obtain voxel features. These features are subsequently compressed along the Z dimension to obtain BEV features. In contrast, Pointpillar (Lang et al., 2019) projects the point cloud into multiple pillars and pools the points within each pillar to extract features for BEV-based detection.

**Temporal-aware 3D Object Detection.** Temporal fusion has emerged as a hot research topic in the field of 3D object detection for its ability to enhance detection stability and perception of target motion. BEVFormer (Li et al., 2022c) uses spatiotemporal attention to fuse the historical BEV features of the previous frame with current image features. BEVDet4D (Huang & Huang, 2022) employs concatenation to fuse temporally aligned BEV features from adjacent frames. SOLOFusion (Park et al., 2022) further leverages this approach to achieve long-term temporal fusion. Some methods perform temporal information fusion directly on the original feature sequences based on query. For instance, PETRv2 (Liu et al., 2022b) employs global attention and temporal position encoding to fuse temporal information, while Sparse4D (Lin et al., 2022) models the relationship between multiple frames based on sparse attention. Additionally, StreamPETR (Wang et al., 2023b) introduces a method for long-term fusion by leveraging object queries from past frames.

**Multi-modal 3D Object Detection.** Fusing multi-sensory features becomes a de-facto standard in 3D perception tasks. BEVFusion-based methods (Liu et al., 2023; Liang et al., 2022; Cai et al., 2023) obtain image BEV features using view transform (Phillion & Fidler, 2020; Li et al., 2022c) and concatenates them with LIDAR BEV features via simple concatenation. However, such simple stragety may fail to fully exploit the complementary information between multi-modal features. Another line of approaches construct transformer (Bai et al., 2022; Wang et al., 2023a; Yang et al., 2022) based architectures to perform interaction between image and point-cloud features. These methods relies simultaneously on both image and point cloud modal features, which presents challenges in cases of robustness scenarios when missing a modality data. Concurrently, Yan et al. (2023) proposes a method, dubbed CMT, which adopts 3D position encoding to achieve end-to-end multimodal fusion-based 3D object detection using transformer. Nonetheless, the aforementioned fusion methods rely

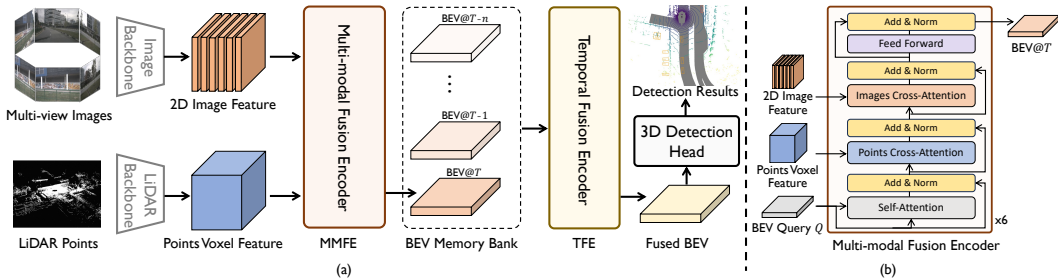


Figure 2: **(a) The framework of the FusionFormer.** The LiDAR point cloud and multi-view images are processed separately in their respective backbone networks to extract voxel features and image features. These features are then inputted into a multi-modal fusion encoder (MMFE) to generate the fused BEV features. The fused BEV features of the current frame, along with the BEV features from historical frames, are jointly fed into a temporal fusion encoder (TFE) to obtain the multi-modal temporal fused BEV features. Finally, the features are utilized in the detection head to produce the final 3D object detection results. **(b) The architecture of the Multi-modal Fusion Encoder (MMFE).** The BEV queries are initialized and subsequently subjected to self-attention. They are then sequentially utilized for cross-attention with the point cloud voxel features and image features. The resulting BEV queries, updated through a feed-forward network, are propagated as inputs to the subsequent encoder layers. Following multiple layers of fusion encoding, the ultimate fused BEV feature is obtained.

on compressing point cloud voxel features into BEV representations, which can result in the loss of the height information. To tackle this, UVTR (Li et al., 2022b) introduced knowledge transfer to perform voxel-level multi-modal fusion by directly combining LiDAR voxel features with image voxel features obtained through LSS. However, this approach did not yield notable improvements in performance. Unlike these approaches, FusionFormer demonstrates enhanced adaptability to the input format of multimodal features, allowing direct utilization of point cloud features in voxel form. Moreover, by incorporating deformable attention and residual structures within the fusion encoding module, FusionFormer can achieve both multimodal feature complementarity and robustness in handling missing modal data.

### 3 METHOD

Here we present our method in detail. Figure 2 (a) illustrates our proposed FusionFormer for multimodal temporal fusion. By utilizing a fusion encoder based on deformable attention (Lin et al., 2022), LiDAR and image features are transformed into fused BEV features. Compared to previous approaches such as BEVFusion (Liu et al., 2023; Liang et al., 2022), FusionFormer can adapt to different feature representations of different modalities without requiring pre-transformation into BEV space. The image branch can retain its original 2D feature representation, while the point cloud branch can be represented as BEV features or voxel features. Detailed information regarding the image branch and point cloud branch can be found in the A.1 section of the appendix. The temporal fusion module utilizes deformable attention to fuse BEV features from the current and previous frames that have been temporally aligned. Then the processed multimodal temporal fusion BEV features are input into the detection task head to obtain 3D object detection results.

#### 3.1 MULTI-MODAL FUSION ENCODER

As illustrated in Figure 2 (b), the fusion encoding module consists of 6 layers, each incorporating self-attention, points cross-attention, and images cross-attention. In accordance with the standard transformer architecture, the BEV queries are subjected to self-attention following initialization. Subsequently, points cross-attention is executed to facilitate the integration of LiDAR features, which is further enhanced through images cross-attention to fuse image features. The encoding layer outputs the updated queries as input to the next layer after being processed through a feed-forward network. After 6 layers of fusion encoding, the final multimodal fusion BEV features are obtained.

**BEV Queries.** We partition the BEV space within the surrounding region of interest (ROI) range around the vehicle’s center into a grid of  $H \times W$  cells. Correspondingly, we define a set of learnable parameters  $Q$  to serve as the queries for the BEV space. Each  $q$  corresponds to a cell in the BEV space. Prior to inputting  $Q$  into the fusion encoder, the BEV queries are subjected to position encoding based on their corresponding BEV spatial coordinates (Li et al., 2022c).

**Self-Attention.** To reduce computational resource usage, we implemented the self-attention based on deformable attention. Each BEV query interacts only with its corresponding queries within the ROI range. This process is achieved through feature sampling at the 2D reference points for each query as illustrated below:

$$SA(Q_p) = DefAttn(Q_p, p, Q) \quad (1)$$

where  $Q_p$  represents the BEV query at point  $p = (x, y)$ .

**Points Cross-Attention.** The points cross-attention layer is also implemented based on deformable attention, but the specific manner in which points cross-attention is implemented varies depending on the form of the LiDAR points features. For the case where BEV features are used as input, we implement the points cross-attention layer as follows:

$$PCA_{2D}(Q_p, B_{pts}) = DefAttn(Q_p, P_{2D}, B_{pts}) \quad (2)$$

where  $B_{pts}$  represents the BEV features output by the LiDAR branch, and  $P_{2D} = (x_{2D}, y_{2D})$  represents the 2D projection of the coordinate  $p = (x, y)$  onto the point cloud BEV space.

For the case where voxel features are used as input, the points cross-attention layer is implemented as follows:

$$PCA_{3D}(Q_p, V_{pts}) = \sum_{i=1}^{N_{ref}} DefAttn(Q_p, P_{3D}(p, i), V_{pts}) \quad (3)$$

where  $V_{pts}$  represents the voxel features output by the LiDAR branch.

To obtain the 3D reference points, we first expand the grid cell corresponding to each BEV query with a height dimension, similar to the pillar representation (Lang et al., 2019). Then, from each pillar corresponding to a query, we sample a fixed number of  $N_{ref}$  reference points, which are projected onto the point cloud voxel space using the projection equation  $P_{3D}$ . Specifically, for each query located at  $p = (x, y)$ , a set of height anchors  $\{z_i\}_{i=1}^{N_{ref}}$  are defined along its  $Z$ -axis. Consequently, for each BEV query  $Q_p$ , a corresponding set of 3D reference points  $(x, y, z_i)_{i=1}^{N_{ref}}$  is obtained. And the projection equation is as follow:

$$P_{3D}(p, i) = (x_{pts}, y_{pts}, z_{pts}) \quad (4)$$

where  $P_{3D}(p, i)$  is the projection of the  $i$ -th 3D reference point of BEV query  $Q_p$  in the LiDAR space.

**Images Cross-Attention.** The implementation of the images cross-attention is similar to the points cross-attention with voxel features as input. Since the images have multi views, the 3D reference points of each query can only be projected onto a subset of the camera views. Following BEV-Former (Li et al., 2022c), we denote the views that can be projected as  $V_{hit}$ . Therefore, the images cross-attention process can be expressed as:

$$ICA(Q_p, F) = \frac{1}{V_{hit}} \sum_{i=1}^{N_{ref}} \sum_{j=1}^{V_{hit}} DefAttn(Q_p, P(p, i, j), F_j) \quad (5)$$

where  $j$  is the index of the camera view,  $F_j$  represents the image features of the  $j$ -th camera, and  $P(p, i, j)$  represents the projection point of the  $i$ -th 3D reference point  $(x, y, z_i)$  of query  $Q_p$  in the image coordinate system of the  $j$ -th camera.

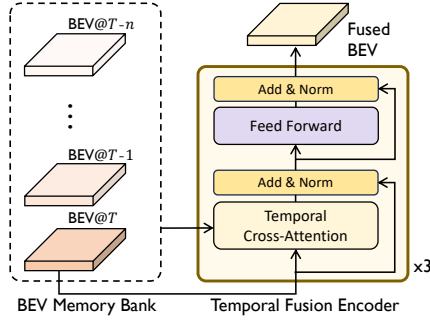


Figure 3: **Temporal Fusion Encoder (TFE).** The initial set of BEV queries is formed by utilizing the BEV features of the current frame. These queries are then subjected to cross-attention with historical BEV features, including the current frame. The resulting queries are updated through a feed-forward network and serve as inputs for the subsequent layer. Through multiple layers of temporal fusion encoding, the final output is obtained, representing the temporally fused BEV feature.

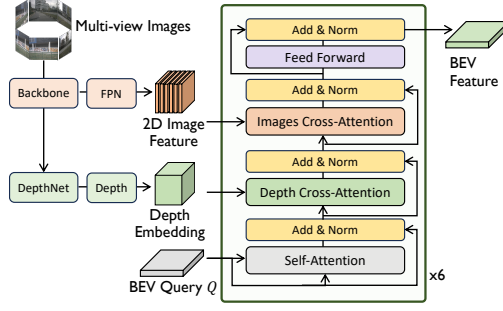


Figure 4: **Fusion with depth prediction.** After being processed by the backbone network, the multi-view image features are split into two branches. One branch utilizes a feature pyramid network (FPN) to extract multi-scale image features. The other branch employs a monocular depth prediction network to estimate depth and utilizes 3D convolution to encode the depth predictions. The multi-scale image features and the depth embedding are jointly input into the encoder to obtain the BEV features.

### 3.2 TEMPORAL FUSION ENCODER

As shown in Figure 3, the temporal fusion encoder (TFE) consists of three layers, each comprising BEV temporal-attention and feedforward networks. At the first layer, the queries are initialized with the BEV features of the current frame and then updated through temporal-attention using historical BEV features. The resulting queries are passed through a feedforward network and serve as input to the next layer. After three layers of fusion encoding, the final temporal fusion BEV features are obtained. The temporal-attention process can be expressed as:

$$TCA(Q_p, B) = \sum_{i=0}^T DefAttn(Q_p, P, B_{t-i}) \quad (6)$$

where  $B_{t-i}$  represents the BEV feature at time  $t - i$ .

### 3.3 FUSION WITH DEPTH PREDICTION

The flexibility of FusionFormer enables us to approximate the point cloud branch in scenarios where only camera images are available by adding an image-based monocular depth prediction branch. As illustrated in Figure 4, we propose a depth prediction network to generate interval-based depth predictions from input image features. 3D convolution is utilized to encode the depth prediction results as voxel features in each camera frustum. Depth cross-attention is then employed to fuse the depth features. The process of depth cross-attention is defined as follows:

$$DCA(Q_p, D) = \frac{1}{V_{hit}} \sum_{i=1}^{N_{ref}} \sum_{j=1}^{V_{hit}} DefAttn(Q_p, P(p, i, j), D_j) \quad (7)$$

where  $D_j$  denotes the encoded depth prediction features of the  $j$ -th camera, and  $P(p, i, j)$  represents the projection point of the  $i$ -th 3D reference point  $(x, y, z_i)$  of query  $Q_p$  onto the frustum coordinate system of the  $j$ -th camera.

## 4 EXPERIMENTS

This section presents the performance of our proposed FusionFormer on the task of 3D object detection, along with several ablation studies that analyze the benefits of each module in our framework.

Table 1: Performance comparison on the nuScenes test set. "L" is LiDAR. "C" is camera. "T" is temporal. The results are evaluated using a single model without any test-time-augmentation or ensembling techniques.

Methods	Modality	NDS $\uparrow$	mAP $\uparrow$	mATE $\downarrow$	mASE $\downarrow$	mAOE $\downarrow$	mAVE $\downarrow$	mAAE $\downarrow$
PointPainting(Vora et al.)	CL	61.0	54.1	38.0	26.0	54.1	29.3	13.1
PointAugmenting(Wang et al.)	CL	71.1	66.8	25.3	<b>23.5</b>	35.4	26.6	12.3
MVP(Chen et al.)	CL	70.5	66.4	26.3	23.8	32.1	31.3	13.4
FusionPainting(Xu et al.)	CL	71.6	68.1	25.6	23.6	34.6	27.4	13.2
TransFusion(Bai et al.)	CL	71.7	68.9	25.9	24.3	35.9	28.8	12.7
BEVFusion(Liu et al.)	CL	72.9	70.2	26.1	23.9	32.9	26.0	13.4
BEVFusion(Liang et al.)	CL	73.3	71.3	<b>25.0</b>	24.0	35.9	25.4	13.2
UVTR(Li et al.)	CL	71.1	67.1	30.6	24.5	35.1	<b>22.5</b>	12.4
CMT(Yan et al.)	CL	74.1	72.0	27.9	<b>23.5</b>	30.8	25.9	11.2
DeepInteraction(Yang et al.)	CL	73.4	70.8	25.7	24.0	32.5	24.5	12.8
BEVFusion4D(Cai et al.)	CLT	74.7	<b>73.3</b>	-	-	-	-	-
FusionFormer	CLT	<b>75.1</b>	72.6	26.7	23.6	<b>28.6</b>	<b>22.5</b>	<b>10.5</b>

Table 2: Performance comparison on the nuScenes val set. "L" is LiDAR. "C" is camera. "T" is temporal. The "-S" indicates that the model only utilizes single-frame BEV features without incorporating temporal fusion techniques. The results are evaluated using a single model without any test-time-augmentation or ensembling techniques.

Methods	Image Backbone	LiDAR Backbone	Modality	mAP $\uparrow$	NDS $\uparrow$
TransFusion(Bai et al.)	DLA34	voxel0075	CL	67.5	71.3
BEVFusion(Liu et al.)	Swin-T	voxel0075	CL	68.5	71.4
BEVFusion(Liang et al.)	Swin-T	voxel0075	CL	67.9	71.0
UVTR(Li et al.)	R101	voxel0075	CL	65.4	70.2
CMT(Yan et al.)	VoV-99	voxel0075	CL	70.3	72.9
DeepInteraction(Yang et al.)	R50	voxel0075	CL	69.9	72.6
BEVFusion4D-S(Cai et al.)	Swin-T	voxel0075	CL	70.9	72.9
BEVFusion4D(Cai et al.)	Swin-T	voxel0075	CLT	<b>72.0</b>	73.5
FusionFormer-S	VoV-99	voxel0075	CL	70.0	73.2
FusionFormer	VoV-99	voxel0075	CLT	71.4	<b>74.1</b>

#### 4.1 EXPERIMENTAL SETUPS

**Datasets and metrics.** We conducted experiments on the nuScenes dataset (Caesar et al., 2020) to evaluate the performance of our proposed method for 3D object detection in autonomous driving. The nuScenes dataset consists of 1.4 million 3D detection boxes from 10 different categories, with each frame of data containing 6 surround-view camera images and LiDAR point cloud data. We employ the nuScenes detection metrics NDS and mAP as evaluation metrics for our experiments.

**Implementation details.** We conducted algorithmic experiments using the open-source project MMDetection3D (Contributors, 2020) based on PyTorch. Specifically, we selected VoVNet-99 (Lee & Park, 2020) as the backbone for the image branch, generating multi-scale image features through FPN (Lin et al., 2017). The input image size was set to  $1600 \times 640$ . For the LiDAR point cloud branch, VoxelNet (Zhou & Tuzel, 2018) was used as the backbone. The input LiDAR point cloud was voxelized with a size of  $0.075m$ . The size of the BEV queries was set to  $200 \times 200$ . During the training process, we loaded the pre-trained weights of the image branch backbone on Fcos3D (Wang et al., 2021b). The point cloud branch did not require pre-trained weights and was directly trained end-to-end with the model. We present a 3D detection head based on Deformable DETR (Zhu et al., 2020) that outputs 3D detection boxes and velocity predictions directly from BEV features without the need for non-maximum suppressing. To address the unstable matching problem encountered in DETR-like detection heads and accelerate training convergence, we applied the query denoising strategy (Li et al., 2022a) during the training process. The model was trained for 24 epochs with the class-balanced grouping and sampling (CBGS) strategy (Zhu et al., 2019).

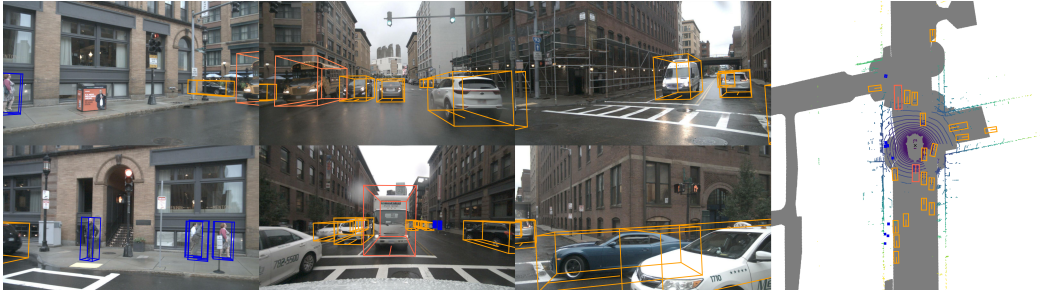


Figure 5: **Qualitative detection results in the nuScenes test set.** Bounding boxes with different colors represent Cars (●), Pedestrians (●), Bus (●) and Truck (●).

#### 4.2 COMPARISON WITH STATE-OF-THE-ART METHODS

As shown in Table 1, FusionFormer achieves 75.1% NDS and 72.6% mAP on the nuScenes test dataset for 3D object detection, outperforming state-of-the-art methods. We used a single model fused with 8 frames of historical BEV features without any test-time-augmentation or ensembling techniques. We also compared the performance of FusionFormer with other methods on the nuScenes val dataset as shown in Table 2. Our proposed FusionFormer achieves state-of-the-art performance on both single-frame and temporal fusion scenarios with NDS scores of 73.2% and 74.1%. Several detection results on the nuScenes test set of FusionFormer are shown in Figure 5.

Table 3: Results of camera based 3D detection fused with depth prediction.

Method	mAP $\uparrow$	NDS $\uparrow$
BEVFormer(Li et al.)	41.6	51.7
FusionFormer-Depth	<b>43.9</b>	<b>53.3</b>

Table 4: Robustness performance on the nuScenes val set. "L" is LiDAR. "C" is camera.

Method	Modality	mAP $\uparrow$	NDS $\uparrow$
FusionFormer	C	34.3	45.5
FusionFormer	L	62.5	68.6
FusionFormer	CL	71.4	74.1

#### 4.3 CAMERA BASED 3D DETECTION FUSED WITH DEPTH PREDICTION

As shown in Table 3, FusionFormer achieves 53.3% NDS and 43.9% mAP on the nuScenes val dataset with only camera images input by fused with the depth prediction results. Compared with the baseline BEVFormer, the NDS and mAP increased by 1.6% and 2.3% respectively. In particular, we found that after introducing the depth prediction branch, the BEV features output by the encoder can converge better. This may be because the depth information carried by the depth prediction branch allows the model to focus more accurately on the target location. As shown in Figure 6 (a), compared to BEVFormer, the BEV features obtained through FusionFormer-Depth are noticeably more focused on the target location.

#### 4.4 ROBUSTNESS STUDY

During the training process, we incorporated modality mask (Yan et al., 2023; Yu et al., 2023) to enhance the model’s robustness to missing modality data. As demonstrated in Table 4, our model can produce desirable results even in scenarios where image or point cloud data is missing, showcasing its strong robustness. These findings highlight the potential of our approach for addressing challenges in multi-modal learning and its potential for practical real-world applications.

#### 4.5 ABLATION STUDY

In this section, we investigate the influence of each module on the performance of our proposed multi-modal fusion model for 3D detection. We adopted ResNet-50 (He et al., 2016) as the backbone for the image branch, with an input resolution of  $800 \times 320$  for the image and a voxel size of  $0.1m$  for the point cloud branch, outputting  $150 \times 150$  BEV features. It is noteworthy that, all the experiments presented in this section were based on single frame without incorporating temporal

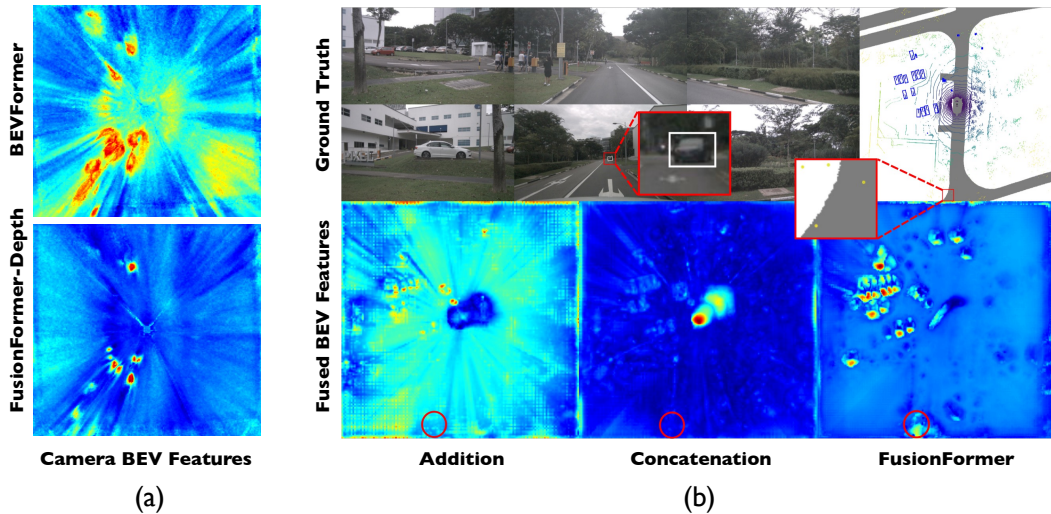


Figure 6: (a) Visualization of the camera BEV features of BEVFormer and FusionFormer-Depth. The BEV features obtained through FusionFormer-Depth are noticeably more focused on the target location than BEVFormer. (b) Illustrations of the fused BEV features of different fusion methods. The car labeled in the image are not annotated in the ground truth because they are far away and the LiDAR captures fewer points. FusionFormer is capable of better integrating multimodal features and can detect distant objects using image information even when the point cloud is sparse.

fusion techniques. The models were trained for 24 epochs without utilizing the CBGS (Zhu et al., 2019) strategy.

**LiDAR Features.** In order to evaluate the impact of fusing voxel features from point cloud, we conducted experiments by comparing the model’s performance with LiDAR features using BEV and voxel representations. Table 5 presents the results of all models. In contrast to inputting LiDAR features in the form of BEV, the use of voxel input format leads to superior model performance. Notably, the prediction errors for object center location and orientation are significantly reduced. This may be attributed to the preservation of more object structural information of the Z-axis in the voxel format, resulting in more accurate detection outcomes.

Table 5: Study for the representation of the LiDAR feature on the nuScenes val set.

LiDAR	mAP $\uparrow$	NDS $\uparrow$	mATE $\downarrow$	mAOE $\downarrow$
BEV	61.3	66.1	35.7	36.9
Voxel	<b>62.7</b>	<b>67.3</b>	<b>34.4</b>	<b>31.4</b>

Table 6: Ablation study of the modality fusion module on the nuScenes val set.

Fusion Method	mAP $\uparrow$	NDS $\uparrow$
Addition	59.3	64.6
concatenation	59.2	64.5
Ours	<b>62.7</b>	<b>67.3</b>

**Modality Fusion.** We conducted a comparative analysis of our proposed modality fusion method with other fusion methods to evaluate their performance. In the case of the fusion methods of addition and concatenation, the image BEV features were obtained through BEVFormer(Li et al., 2022c). The experimental results are presented in Table 6. As shown in Figure 6 (b), compared to other fusion methods, the fused BEV features obtained through FusionFormer exhibit a stronger response to the targets. Specifically, the distant cars labeled in the image are excluded from the ground truth (GT) annotations due to the limited points captured by LiDAR. Consequently, conventional multimodal fusion methods, such as simple addition and concatenation, fail to effectively incorporate these distant objects. In contrast, our proposed method, FusionFormer, enables enhanced fusion of multimodal features. It leverages the complementary information from image data to detect distant objects even in scenarios with sparse point cloud data.

---

## 5 CONCLUSION

In this paper, we propose a novel transformer-based framework with a uniform sampling strategy that overcomes the limitations of existing multi-modality frameworks. Our approach eliminates the need for compressing voxel features into BEV space before fusion with image features, resulting in superior performance. We demonstrate the versatility of our method by transforming it into a camera-only 3D object detector, utilizing image features obtained through monocular depth estimation instead of LiDAR features. Our method achieves state-of-the-art performance in the 3D object detection task on the nuScenes dataset. In future, we will explore the applications of FusionFormer in other tasks, such as map segmentation.

## REFERENCES

- Xuyang Bai, Zeyu Hu, Xinge Zhu, Qingqiu Huang, Yilun Chen, Hongbo Fu, and Chiew-Lan Tai. Transfusion: Robust lidar-camera fusion for 3d object detection with transformers. In Proceedings of the IEEE/CVF conference on computer vision and pattern recognition, pp. 1090–1099, 2022.
- Holger Caesar, Varun Bankiti, Alex H Lang, Sourabh Vora, Venice Erin Liong, Qiang Xu, Anush Krishnan, Yu Pan, Giancarlo Baldan, and Oscar Beijbom. nuscenes: A multimodal dataset for autonomous driving. In Proceedings of the IEEE/CVF conference on computer vision and pattern recognition, pp. 11621–11631, 2020.
- Hongxiang Cai, Zeyuan Zhang, Zhenyu Zhou, Ziyin Li, Wenbo Ding, and Jiuhua Zhao. Bev-fusion4d: Learning lidar-camera fusion under bird’s-eye-view via cross-modality guidance and temporal aggregation. arXiv preprint arXiv:2303.17099, 2023.
- Xiaozhi Chen, Huimin Ma, Ji Wan, Bo Li, and Tian Xia. Multi-view 3d object detection network for autonomous driving. In Proceedings of the IEEE conference on Computer Vision and Pattern Recognition, pp. 1907–1915, 2017.
- Yukang Chen, Jianhui Liu, Xiangyu Zhang, Xiaojuan Qi, and Jiaya Jia. Voxelnex: Fully sparse voxelnet for 3d object detection and tracking. In Proceedings of the IEEE/CVF Conference on Computer Vision and Pattern Recognition, pp. 21674–21683, 2023.
- MMDetection3D Contributors. MMDetection3D: OpenMMLab next-generation platform for general 3D object detection. <https://github.com/open-mmlab/mmdetection3d>, 2020.
- Kaiming He, Xiangyu Zhang, Shaoqing Ren, and Jian Sun. Deep residual learning for image recognition. In Proceedings of the IEEE conference on computer vision and pattern recognition, pp. 770–778, 2016.
- Junjie Huang and Guan Huang. Bevdet4d: Exploit temporal cues in multi-camera 3d object detection. arXiv preprint arXiv:2203.17054, 2022.
- Junjie Huang, Guan Huang, Zheng Zhu, Yun Ye, and Dalong Du. Bevdet: High-performance multi-camera 3d object detection in bird-eye-view. arXiv preprint arXiv:2112.11790, 2021.
- Alex H Lang, Sourabh Vora, Holger Caesar, Lubing Zhou, Jiong Yang, and Oscar Beijbom. Pointpillars: Fast encoders for object detection from point clouds. In Proceedings of the IEEE/CVF conference on computer vision and pattern recognition, pp. 12697–12705, 2019.
- Youngwan Lee and Jongyoul Park. Centermask: Real-time anchor-free instance segmentation. In Proceedings of the IEEE/CVF conference on computer vision and pattern recognition, pp. 13906–13915, 2020.
- Feng Li, Hao Zhang, Shilong Liu, Jian Guo, Lionel M Ni, and Lei Zhang. Dn-detr: Accelerate detr training by introducing query denoising. In Proceedings of the IEEE/CVF Conference on Computer Vision and Pattern Recognition, pp. 13619–13627, 2022a.
- Yanwei Li, Yilun Chen, Xiaojuan Qi, Zeming Li, Jian Sun, and Jiaya Jia. Unifying voxel-based representation with transformer for 3d object detection. Advances in Neural Information Processing Systems, 35:18442–18455, 2022b.

- 
- Yinhao Li, Zheng Ge, Guanyi Yu, Jinrong Yang, Zengran Wang, Yukang Shi, Jianjian Sun, and Zem-ing Li. Bevdepth: Acquisition of reliable depth for multi-view 3d object detection. In Proceedings of the AAAI Conference on Artificial Intelligence, volume 37, pp. 1477–1485, 2023.
- Zhiqi Li, Wenhai Wang, Hongyang Li, Enze Xie, Chonghao Sima, Tong Lu, Yu Qiao, and Jifeng Dai. Bevformer: Learning bird’s-eye-view representation from multi-camera images via spatiotemporal transformers. In European conference on computer vision, pp. 1–18. Springer, 2022c.
- Tingting Liang, Hongwei Xie, Kaicheng Yu, Zhongyu Xia, Zhiwei Lin, Yongtao Wang, Tao Tang, Bing Wang, and Zhi Tang. Bevfusion: A simple and robust lidar-camera fusion framework. Advances in Neural Information Processing Systems, 35:10421–10434, 2022.
- Tsung-Yi Lin, Piotr Dollár, Ross Girshick, Kaiming He, Bharath Hariharan, and Serge Belongie. Feature pyramid networks for object detection. In Proceedings of the IEEE conference on computer vision and pattern recognition, pp. 2117–2125, 2017.
- Xuwu Lin, Tianwei Lin, Zixiang Pei, Lichao Huang, and Zhizhong Su. Sparse4d: Multi-view 3d object detection with sparse spatial-temporal fusion. arXiv preprint arXiv:2211.10581, 2022.
- Yingfei Liu, Tiancai Wang, Xiangyu Zhang, and Jian Sun. Petr: Position embedding transformation for multi-view 3d object detection. In European Conference on Computer Vision, pp. 531–548. Springer, 2022a.
- Yingfei Liu, Junjie Yan, Fan Jia, Shuailin Li, Aqi Gao, Tiancai Wang, Xiangyu Zhang, and Jian Sun. Petr2: A unified framework for 3d perception from multi-camera images. arXiv preprint arXiv:2206.01256, 2022b.
- Zhijian Liu, Haotian Tang, Alexander Amini, Xinyu Yang, Huizi Mao, Daniela L Rus, and Song Han. Bevfusion: Multi-task multi-sensor fusion with unified bird’s-eye view representation. In 2023 IEEE International Conference on Robotics and Automation (ICRA), pp. 2774–2781. IEEE, 2023.
- Michael Meyer and Georg Kusch. Automotive radar dataset for deep learning based 3d object detection. In 2019 16th european radar conference (EuRAD), pp. 129–132. IEEE, 2019.
- Michael Meyer, Georg Kusch, and Sven Tomforde. Graph convolutional networks for 3d object detection on radar data. In Proceedings of the IEEE/CVF International Conference on Computer Vision, pp. 3060–3069, 2021.
- Anshul Paigwar, Ozgur Er kent, Christian Wolf, and Christian Laugier. Attentional pointnet for 3d-object detection in point clouds. In Proceedings of the IEEE/CVF Conference on Computer Vision and Pattern Recognition Workshops, pp. 0–0, 2019.
- Dennis Park, Rares Ambrus, Vitor Guizilini, Jie Li, and Adrien Gaidon. Is pseudo-lidar needed for monocular 3d object detection? In Proceedings of the IEEE/CVF International Conference on Computer Vision, pp. 3142–3152, 2021.
- Jinhyung Park, Chenfeng Xu, Shijia Yang, Kurt Keutzer, Kris Kitani, Masayoshi Tomizuka, and Wei Zhan. Time will tell: New outlooks and a baseline for temporal multi-view 3d object detection. arXiv preprint arXiv:2210.02443, 2022.
- Jonah Philion and Sanja Fidler. Lift, splat, shoot: Encoding images from arbitrary camera rigs by implicitly unprojecting to 3d. In Computer Vision–ECCV 2020: 16th European Conference, Glasgow, UK, August 23–28, 2020, Proceedings, Part XIV 16, pp. 194–210. Springer, 2020.
- Charles R Qi, Wei Liu, Chenxia Wu, Hao Su, and Leonidas J Guibas. Frustum pointnets for 3d object detection from rgb-d data. In Proceedings of the IEEE conference on computer vision and pattern recognition, pp. 918–927, 2018.
- Sourabh Vora, Alex H Lang, Bassam Helou, and Oscar Beijbom. Pointpainting: Sequential fusion for 3d object detection. In Proceedings of the IEEE/CVF conference on computer vision and pattern recognition, pp. 4604–4612, 2020.

- 
- Chunwei Wang, Chao Ma, Ming Zhu, and Xiaokang Yang. Pointaugmenting: Cross-modal augmentation for 3d object detection. In Proceedings of the IEEE/CVF Conference on Computer Vision and Pattern Recognition, pp. 11794–11803, 2021a.
- Haiyang Wang, Hao Tang, Shaoshuai Shi, Aoxue Li, Zhenguo Li, Bernt Schiele, and Liwei Wang. Unitr: A unified and efficient multi-modal transformer for bird’s-eye-view representation. arXiv preprint arXiv:2308.07732, 2023a.
- Jun Wang, Shiyi Lan, Mingfei Gao, and Larry S Davis. Infofocus: 3d object detection for autonomous driving with dynamic information modeling. In Computer Vision–ECCV 2020: 16th European Conference, Glasgow, UK, August 23–28, 2020, Proceedings, Part X 16, pp. 405–420. Springer, 2020.
- Shihao Wang, Yingfei Liu, Tiancai Wang, Ying Li, and Xiangyu Zhang. Exploring object-centric temporal modeling for efficient multi-view 3d object detection. arXiv preprint arXiv:2303.11926, 2023b.
- Tai Wang, Xinge Zhu, Jiangmiao Pang, and Dahua Lin. Fcos3d: Fully convolutional one-stage monocular 3d object detection. In Proceedings of the IEEE/CVF International Conference on Computer Vision, pp. 913–922, 2021b.
- Yue Wang, Vitor Campagnolo Guizilini, Tianyuan Zhang, Yilun Wang, Hang Zhao, and Justin Solomon. Detr3d: 3d object detection from multi-view images via 3d-to-2d queries. In Conference on Robot Learning, pp. 180–191. PMLR, 2022.
- Enze Xie, Zhiding Yu, Daquan Zhou, Jonah Philion, Anima Anandkumar, Sanja Fidler, Ping Luo, and Jose M Alvarez. M<sup>2</sup> bev: Multi-camera joint 3d detection and segmentation with unified birds-eye view representation. arXiv preprint arXiv:2204.05088, 2022.
- Shaoqing Xu, Dingfu Zhou, Jin Fang, Junbo Yin, Zhou Bin, and Liangjun Zhang. Fusionpainting: Multimodal fusion with adaptive attention for 3d object detection. In 2021 IEEE International Intelligent Transportation Systems Conference (ITSC), pp. 3047–3054. IEEE, 2021.
- Junjie Yan, Yingfei Liu, Jianjian Sun, Fan Jia, Shuailin Li, Tiancai Wang, and Xiangyu Zhang. Cross modal transformer via coordinates encoding for 3d object detection. arXiv preprint arXiv:2301.01283, 2023.
- Zeyu Yang, Jiaqi Chen, Zhenwei Miao, Wei Li, Xiatian Zhu, and Li Zhang. Deepinteraction: 3d object detection via modality interaction. Advances in Neural Information Processing Systems, 35:1992–2005, 2022.
- Tianwei Yin, Xingyi Zhou, and Philipp Krahenbuhl. Center-based 3d object detection and tracking. In Proceedings of the IEEE/CVF conference on computer vision and pattern recognition, pp. 11784–11793, 2021.
- Kaicheng Yu, Tang Tao, Hongwei Xie, Zhiwei Lin, Tingting Liang, Bing Wang, Peng Chen, Dayang Hao, Yongtao Wang, and Xiaodan Liang. Benchmarking the robustness of lidar-camera fusion for 3d object detection. In Proceedings of the IEEE/CVF Conference on Computer Vision and Pattern Recognition, pp. 3187–3197, 2023.
- Yin Zhou and Oncel Tuzel. Voxelnet: End-to-end learning for point cloud based 3d object detection. In Proceedings of the IEEE conference on computer vision and pattern recognition, pp. 4490–4499, 2018.
- Benjin Zhu, Zhengkai Jiang, Xiangxin Zhou, Zeming Li, and Gang Yu. Class-balanced grouping and sampling for point cloud 3d object detection. arXiv preprint arXiv:1908.09492, 2019.
- Xizhou Zhu, Weijie Su, Lewei Lu, Bin Li, Xiaogang Wang, and Jifeng Dai. Deformable detr: Deformable transformers for end-to-end object detection. arXiv preprint arXiv:2010.04159, 2020.

---

## A APPENDIX

### A.1 MULTI-MODAL BRANCHES

**Camera Branch.** To extract image features from multi-view camera images, a backbone network, such as ResNet-50, is employed. These image features are then processed by a feature pyramid network (FPN), which generates multi-scale image features.

**LiDAR Branch.** FusionFormer is designed to accommodate diverse representations of multi-modal features. This study explores two different representation forms of LiDAR features, specifically BEV and voxel features. The original point cloud data is voxelized, and then processed through sparse 3D convolution operations. In one case, voxel features are obtained by encoding the volumetric representation using 3D convolution operations. In another case, the Z-axis of the features are compressed into the channel dimension, and BEV features are obtained with 2D convolution operations.

### A.2 EFFICIENCY STUDY

As shown in Table 7, we compare the efficiency of FusionFormer and existing methods. The FPS and performance are tested on a single Tesla A100 GPU with the best model setting of official repositories. In comparison to BEVFusion, FusionFormer demonstrates superior performance with notable improvements of 3.1% in mAP and 2.7% in NDS, while maintaining a similar processing speed. These results highlight the significant advancements achieved by FusionFormer in the field of object detection.

Table 7: Efficiency comparison on the nuScenes val set. "L" is LiDAR. "C" is camera. "T" is temporal. The "-S" indicates that the model only utilizes single-frame BEV features without incorporating temporal fusion techniques.

Methods	Modality	mAP $\uparrow$	NDS $\uparrow$	FPS
TransFusion	CL	67.5	71.3	3.2
BEVFusion	CL	68.5	71.4	4.2
UVTR	CL	65.4	70.2	2.6
CMT	CL	70.3	72.9	<b>6.0</b>
DeepInteraction	CL	69.8	72.6	1.7
FusionFormer-S	CL	70.0	73.2	4.0
FusionFormer	CLT	<b>71.4</b>	<b>74.1</b>	3.8

### A.3 QUALITATIVE DETECTION RESULTS

In this section, we showcase further detection results of FusionFormer on the nuScenes test set. As depicted in Figure 7, FusionFormer exhibits exceptional performance in detecting objects at long distances. Notably, the incorporation of the temporal fusion module enables FusionFormer to effectively recall occluded objects by leveraging the fused historical frame BEV features. This capability proves valuable in scenarios where objects may be partially or fully obstructed. The presented results highlight the robustness and effectiveness of FusionFormer in addressing the challenges of object detection in complex environments.

### A.4 ADDITIONAL ABLATION STUDY

In this section, we investigate the influence of other factors on the performance of FusionFormer. We adopt ResNet-50 as the backbone for the image branch, with an input resolution of  $800 \times 320$  for the image and a voxel size of  $0.1m$  for the point cloud branch, outputting  $150 \times 150$  BEV features. With the exception of the temporal fusion section, all other experiments presented in this section are based on single frame.



Figure 7: **More qualitative detection results in the nuScenes test set.** Bounding boxes with different colors represent Cars(●), Pedestrians(●), Bus(●) and Truck(●).

**Temporal Fusion.** We conducted a comparative study between our proposed temporal fusion module and the concatenation method used by prior temporal fusion approaches under different temporal sequences. All models were trained for 24 epochs and the CBGS strategy was employed during the training process. The experimental results are presented in Table 8. Compared to the previous temporal fusion method using channel concatenation, our deformable attention-based temporal fusion method demonstrates better performance in 3D object detection.

**CBGS.** We evaluated the impact of utilizing the class-balanced grouping and sampling (CBGS) strategy during the training process on the model’s performance. Table 9 presents the results of this comparison. The application of the CBGS strategy resulted in a balanced distribution of samples across different categories, leading to a notable enhancement in the performance of the model.

**Modality Order.** In our proposed method, multi-modal features are sequentially fed into the fusion encoder at each layer. To evaluate the impact of the input order of multi-modal features, we compared the performance of the model with different input orders. The results are presented in Table 10. All models were trained for 24 epochs without utilizing the CBGS strategy.

**Voxel Size.** We conducted an experiment to evaluate the impact of voxel size on the performance of our proposed method. The results are presented in Table 11. The models were trained for 24 epochs and did not use the CBGS strategy.

**Image Size.** We conducted an experiment to evaluate the impact of image size on the performance of our proposed method. The results are presented in Table 12. The models were trained for 24 epochs and did not use the CBGS strategy.

Table 8: Study of the temporal fusion module on the nuScenes val set.

T	Concate		Ours	
	mAP↑	NDS↑	mAP↑	NDS↑
1	66.48	70.39	66.48	70.39
2	67.71	71.01	67.85	71.20
4	68.18	71.36	68.24	71.51
8	68.31	71.49	68.56	71.66

Table 9: Ablation study of the CBGS strategy on the nuScenes val set.

CBGS	mAP↑	NDS↑
✓	66.5	70.4
	62.7	67.3

Table 10: Ablation study of the input order of modality features on the nuScenes val set.

Order	mAP↑	NDS↑
LC	62.7	67.3
CL	62.5	67.1

Table 11: Ablation study of the voxel size on the nuScenes val set.

Voxel size	mAP↑	NDS↑
0.075m	63.2	67.8
0.100m	62.5	67.1

Table 12: Ablation study of the image size on the nuScenes val set.

Image size	mAP↑	NDS↑
1600×600	64.4	68.1
800×320	62.5	67.1